Optimal site-centered electronic structure basis set from a displaced-center expansion: Improved results via *a priori* estimates of saddle points in the density

Aftab Alam and D. D. Johnson
Department of Materials Science and Engineering, University of Illinois, Urbana-Champaign, Illinois 61801, USA
(Received 13 March 2009; revised manuscript received 12 June 2009; published 24 September 2009)

Site-centered, electronic-structure methods use an expansion inside nonoverlapping "muffin-tin" (MT) spheres plus an interstitial basis set. As the boundary separating the more spherical from nonspherical density between atoms, the "saddle-point" radii (SPR) in the density provide an optimal spherical region for expanding in spherical harmonics, as used in augmented plane wave, muffin-tin orbital, and multiple-scattering [Korringa, Kohn, and Rostoker (KKR)] methods. These MT-SPR guarantee unique, convex Voronoi polyhedra at each site, in distinction to Bader topological cells. We present a numerically fast, two-center expansion to find SPR *a priori* from overlapping *atomic* charge densities, valid also for disordered alloys. We adopt this MT-SPR basis for KKR in the atomic sphere approximation and study (dis)ordered alloys with large differences in atomic size (fcc CoPt and bcc CrW). For this simple and unique improvement, we find formation energies and structural parameters in strikingly better agreement with more exact methods or experiment, and resolve issues with former results.

DOI: 10.1103/PhysRevB.80.125123 PACS number(s): 71.15.Ap, 71.15.Nc, 71.23.−k

Popular site-centered, all-electron, electronic-structure methods, such as augmented plane wave (APW), linear muffin-tin orbital (LMTO), and multiple-scattering theory from Korringa, Kohn, and Rostoker (KKR), use a spherical harmonic expansion of the electronic density and potential in a region defined by nonoverlapping MT spheres, with an additional basis set in the interstitial. Such radii are often arbitrarily chosen, or adjusted by hand, to help, for example, optimize an LAPW basis, better represent the elemental sizes of the atoms, or reduce overlap error in atomic sphere approximation (ASA) calculation. For ASA calculations of ordered and disordered alloys, spheres have been adjusted often with no rigorous basis. It would be beneficial to have a physics-based, closed-form expression that yields, before any calculation, the site-centered basis sets providing the optimal spherical regions to expand, eliminates human intervention, reduces the size of the basis sets, and improves fast but approximate calculations, such as the ASA.

We provide a numerically fast, displaced-center expansion for spherical harmonics (Sec. II) that is applicable to arbitrary number of sublattices and components, as well as the coherent potential approximation (CPA). The expansion is especially useful with *overlapping atomic* charge densities via a Herman-Skillman[1] approach to find *a priori* (i) initial potentials via Löwdin construction,[2] and (ii) the MT, saddle-point radii (SPR) at each site. The MT-SPR reflect an optimal boundary separating the spherical and nonspherical density between neighboring atoms, which improves the representation (as we verify by direct variation), reduces the required basis set [the maximum number of angular momenta, $L_{\max} \equiv (l,m)$], and defines the convex Vornoi polyhedra (Sec. I). As spherical potential methods are ubiquitous due to computational efficacy and relative accuracy, we focus on how the SPR basis dramatically improves the ASA. So, we have implemented the SPR basis in a KKR-CPA-ASA code (Sec. III) and studied (Sec. IV) (dis)ordered alloys with large differences in atomic size (fcc CoPt and bcc CrW) or large c/a distortions (hcp Ti_3Al). We show that the MT-SPR-ASA energies and structural parameters agree strikingly better with full-potential methods and/or measurements, and there is much reduced sensitivity on $L_{\max}$. Also, we show that former "bad" CPA results were not due to issues with the CPA but, rather, due to the poorly represented densities and potentials used. In addition, site excess charges are now more those expected from electronegativity.

I. BACKGROUND

Wigner-Seitz cells in electronic-structure calculations are usually geometrically constructed, convex Voronoi polyhedra (VP),[3] with no reference to the topology of the charge density. As long as basis expansions are done to high enough order and the integrals are done with enough accuracy (both increase computational effort), answers are correct. An improvement to this standard approach would be to use the topology of the charge density to guide the choice of the cell around an atomic site. As evidenced in the calculated charge density of B2 CrW, see Fig. 1, the site-dependent MT spheres (red circles) defined by saddle points in the density (obtained from the application of the expansion here within) reflect the boundary separating the more spherical and nonspherical density between neighboring atoms. Visually apparent are the *s*- and *d*-like character of the W density, where on the same scale (due to spatial extent of density) the contour lines for Cr are closely spaced but completely enclosed by the MT-SPR. Hence, these MT-SPR are physically appropriate and unique choice for the optimal region for expanding in spherical harmonics.

From applied math, we know that touching, inscribed MT spheres guarantee *convex* VP if weights for their construction are chosen as the squares of the MT radii.[4–6] This method is also called *radical plane construction*[4,7] and has been used, e.g., for void formation in unequal spheres[7,8] or nonspherical particles.[9] These generalized Wigner-Seitz cells are called power diagrams,[6,10,11] which can be computed in order $n \log n$ time for n sites in three dimensions.[6,10,12] Such con-

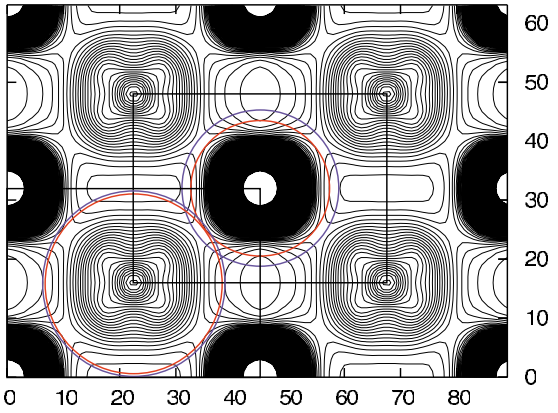

FIG. 1. (Color online) Charge density contours in (110) plane for B2 CrW with a_0=3.016 Å. More spherical versus nonspherical density is evident, with reference to the MT-SPR (red) of 1.1952 Å (1.4238 Å) for small Cr (large W). Volume-conserving ASA radii (the larger, blue circles) of 1.3791 Å (1.5781 Å) are shown. The ratio of larger to smaller MT-SPR (ASA radii) is 1.191 (1.144). Cr- or W-centered unit cell boundaries are given (rectangles). Contour levels are every 0.023 eV/Å^3.

vex VP are also required in KKR to define the single-site scattering matrices,[13,14] such that electron scattering at a site is completed before occurring at a neighboring site. Now, because MT-SPR reflect the spatial extent of the site density (or the atom's "size") and the optimal region for expanding in spherical harmonics, the VP weights should be determined from MT-SPR. In contrast, equal spheres manifestly lead to large nonspherical components in the MT of the smaller atom, as evident in Fig. 1. For B2 CrW, the ratio of the W and Cr MT-SPR spheres is 1.191, and, therefore, due to the power diagram weighting, the ratio of the VP volumes of W and Cr is then $(1.191)^2$. Alternatively, the MT-SPR spheres are 19% different in size, and, thus, the VP volume of W (Cr) increases (decreases) by 19% over the equal sphere case. We are unaware of the use of saddle points in the density to control size and shape of the VP cell to better represent the system in density-functional theory (DFT) calculations. Elsewhere, we will report on the use of isoparametric methods for numerically efficient integration of quantities over each VP without recourse to "shape functions."[13–16]

Using topology of the charge density to improve site-related descriptions is not new. Bader's topological cells are based on the set of extrema (saddle points, maxima and minima) in the density in molecules or solids.[17,18] However, due to the nature of the density, the topological cells exhibit both convex and concave surfaces, making a decidedly inappropriate cell for use in site-centered expansions. Nonetheless, integrating the charge in the topological cells (a post-processing exercise) yields the so-called "Bader charge"[19,20] that more closely follows one's expectation from electronegativity.[17] Yet, the excess charges in MT-SPR derived VP cells (or their approximates, such as ASA) might also be expected to follow physical expectations. Charge difference have been compared between Bader, Mülliken, and Voronoi definitions of spatial integrations.[21] However, Voronoi charges were determined only from the standard geometric definition.

With the MT-SPR in hand, we can obtain the unique set of convex VP (using set of FORTRAN codes adapted from Bernal[22,23]) or ASA spheres at each site. Thus, an efficient, site-shifted (spherical harmonic) expansion would be useful to determine the MT-SPR via saddle points in the atomic overlapping charge density prior to any calculation and to provide a better representation for dramatically improved results for the ASA. In LAPW, some adjustments of the MT spheres (often by hand) are done to help optimize the basis. In ASA calculations, the spheres (whatever their sizes) must fill all space on average. In general, equal spheres are used to minimize the error due to geometrical overlap. However, for systems with atoms of very different sizes, this choice leads to large errors in the total energy, where, e.g., in LMTO, combined correction[24–27] are needed to help ameliorate such errors, which have not been developed for CPA case. Some errors can be reduced by using empty spheres.[25,28]

Attempts have been made to improve ASA approaches. For example, the LMTO total energy of ordered alloys has been minimized with respect to the ASA radii.[29] As the ASA radius is not a variational parameter, such calculations can be unreliable, leading to uncontrolled error and increased sphere overlap. Masuda-Jindo and Terakura[30] used ASW to study strengthening in Al-Li with ASA spheres adjusted according to first-order perturbation analysis of the electron-ion pseudopotential;[31] so the ASA spheres were not equal, but dependent upon ratio of bulk moduli and relative volumes (ASA radii) of the elements. Similarly, Kootte *et al.*[32] studied Co-Pt using ASW by fixing the size of Co spheres from hcp-Co results and then adjusted Pt spheres to conserve volume. In addition, charge transfer depends upon how space is partitioned around each atom. Therefore, equivolume calculations introduce unphysical charge-transfer effects, affecting energetics. Some schemes have been proposed[33–36] to treat these effects in CPA disordered alloys. Singh and Gonis[36] proposed use of charge-neutral ASA spheres, leading to, in some cases, unphysical drops in formation energies. Although untested in detail, Andersen *et al.*[37] proposed making the potential continuous across the sphere boundary by adjusting the ASA radii. In one case, Jepsen and Andersen[38] used saddle points in the spherically averaged (Hartree-only) potential to establish the MT sphere radii, with ASA sphere radii found by scaling up the MT sphere radii equally to conserve cell volume and then adjusted by hand to minimize overlap; however, no publications detail how saddle points were determined, nor what improvements resulted. Although a first-order perturbation analysis of the electron-ion pseudopotential yields a more intricate expression in the impurity limit,[30] the subtlety of adjusting spheres without a physical principle can be seen as follows. Equating the electronic pressure on two ASA spheres one finds that

$$\frac{\Delta V_1}{\Delta V_2} \equiv \frac{V_1 - V_1^0}{V_2 - V_2^0} = \frac{B_2^0}{B_1^0},$$

with the additional requirement of volume conservation. Hence, if volume (V^0) and bulk moduli (B^0) of the elements are similar, then the change to ASA volumes (V) are small; whereas, if the B^0 are quite different (e.g., Al-Li), then ASA

volumes can be adjusted larger at the expense of the element with smallest B^0, lowering the ASA energy unphysically. Saddle-point radii are unique and encompass the correct physical representation.

II. FORMALISM

To achieve an optimized basis set representation via the saddle points in the atomic overlapping charge density, we desire a two-center expansion to calculate the charge density (as well as potential) of the central atom at $\mathbf{r}=0$ and that from the neighboring atoms by shifting the overlapping atomic charge densities to a common origin. To our knowledge, a number of such expansion formulas have been derived (but efficiency is key) and used with different motivations, such as to compute molecular integrals between atomic orbitals about separated centers.[39,40] We apply Löwdin's idea[2,39,40] of spherical harmonic expanding any three-dimensional function $f(\mathbf{r}-\mathbf{R})=f(|\mathbf{r}-\mathbf{R}|)Y_{LM}(\theta_R,\phi_R)$ at a site centered at $\mathbf{r}=\mathbf{R}$ about that at $\mathbf{r}=0$, i.e.,

$$f(\mathbf{r}-\mathbf{R})=\sum_{l=0}^{\infty}\sum_{m=-l}^{+l}\mathcal{V}(l,m;L,M;r,R)Y_{lm}(\theta,\phi), \tag{1}$$

where $Y_{LM}(\theta_R,\phi_R)$ and $Y_{lm}(\theta,\phi)$ are the spherical harmonics around their respective centers, and Ω_R represents the solid angles (θ_R,ϕ_R). We utilize such formulas with the goal of finding an approximate total charge density and locating, *a priori* to any electronic-structure calculation, the saddle points of said density for optimal site-centered basis, for any configuration and even approximations to the disordered state.

The saddle points around each site can be located as the minima in the local total density (Hartree part) along the lines connecting each near-neighbor atom. We define the distance to the closest saddle point at each site as the MT-SPR. Inside this region, we expand wave functions, potentials, and densities in Y_{lm}, as it separates the mostly *spherical density* from the symmetry-induced, nonspherical part in the interstitial; see Fig. 1. The MT-SPR basis better reflect the local charge on a site, more akin to that expected from electronegativities.

Various ways[41–44] have been proposed for deriving such formulas, though not always numerically efficient. One well-known expansion was given by Sack,[45–47] whose early work gave an expansion for $\Psi(r)=r^n$, yielding a series expansions for $\mathcal{V}$. Subsequently, Sack[47] gave $\mathcal{V}$ as an integral, whose kernel, however, must first be found from $\Psi(r)$ by solving an integral equation. We shall use a general method from Silverstone[39] and Suzuki[40] for obtaining the *radial function* $\mathcal{V}$ of Eq. (1) derived from the Fourier-transform convolution theorem. All the quantities in this later approach are formulated in terms of explicit one-dimensional integrals, and we reproduce some equation for completeness and clarity.

Using orthogonality of Y_{LM}, Eq. (1) yields

$$\mathcal{V}(l,m;L,M;r,R)=\int d\Omega f(\mathbf{r}-\mathbf{R})Y^*_{lm}(\Omega). \tag{2}$$

We can cast $\mathcal{V}$ as an overlap integral by introducing a radial function $r^{-2}\delta(r'-r)$ and integrating with respect to $\mathbf{r}'$ on the right-hand side of Eq. (2),

$$\mathcal{V}(lm;LM;r,R)=\int d^3r'\Phi^*(\mathbf{r}')f(\mathbf{r}'-\mathbf{R}), \tag{3}$$

where

$$\Phi(\mathbf{r}')=r^{-2}\delta(r'-r)Y_{lm}(\theta',\phi'). \tag{4}$$

The R dependence of Eq. (3) is greatly simplified by the use of the Fourier-transform convolution theorem[48,49] as

$$\mathcal{V}(lm;LM;r,R)=\frac{1}{(2\pi)^3}\int d^3k\bar{\Phi}^*(\mathbf{k})\bar{f}(\mathbf{k})e^{i\mathbf{k}.\mathbf{R}}. \tag{5}$$

The transforms $\bar{\Phi}(\mathbf{k})$ and $\bar{f}(\mathbf{k})$ can be evaluated conveniently via Bauer's identity,

$$e^{i\mathbf{k}\cdot\mathbf{r}}=\sum_{l=0}^{\infty}\sum_{m=-l}^{+l}4\pi i^l j_l(\kappa r)Y_{lm}(\Omega_k)Y^*_{lm}(\Omega), \tag{6}$$

where $\Omega_k=(\theta_k,\phi_k)$ are the spherical polar coordinate of $\mathbf{k}$ and j_l is the spherical (lth order) Bessel function.

After some effort, a simplified expression for $\mathcal{V}$ in Eq. (5) is obtained, which when substituted back in Eq. (1),[39,40] yields the following form of the site-shifted $f(\mathbf{r}-\mathbf{R})$:

$$f(\mathbf{r}-\mathbf{R})=\sum_{l=0}^{\infty}\sum_{\eta=|L-l|}^{|L+l|}V_{l\eta L}(r,R)\sum_{m=-l}^{+l}C^{\eta}_{LM;lm}Y_{\eta,M-m}(\Omega_R)Y_{lm}(\Omega). \tag{7}$$

Here $C^{\eta}_{LM;lm}$ are Gaunt coefficients defined as

$$C^{\eta}_{LM;lm}=\int d\Omega_k Y^*_{\eta,M-m}(\Omega_k)Y^*_{lm}(\Omega_k)Y_{LM}(\Omega_k). \tag{8}$$

$C^{\eta}_{LM;lm}$ is nonzero if $(\eta+l+L)$ is even. Also $V_{l\eta L}(r,R)$, the radial part of f, has a simple form as the sum of one-dimensional integral, i.e.,

$$V_{l\eta L}(r,R)=\frac{2\pi}{R}(-1)^l\sum_{s=0}^{(L+\eta+l)/2}\sum_{t=0}^{(L+\eta+l)/2-s}D_{l\eta Lst}\left(\frac{r}{R}\right)^{2t-l-1}\times\int_{|r-R|}^{|r+R|}dr'f(r')\left(\frac{r'}{R}\right)^{2s-L+1}. \tag{9}$$

Here, as defined by Silverstone,[39]

$$D_{l\eta Lst}=[(2s)!!(2s-2L-1)!!(2t)!!(2t-2l-1)!!(L+l+\eta-2s-2t)!!(L+l-\eta-2s-2t-1)!!]^{-1}, \tag{10}$$

where the symbol !! indicates a double factorial with a non-negative argument, where $(-1)!!\equiv 1$, while !! allows (non-) negative argument, i.e., for integer n,

$$(2n-1)!!=\begin{cases}(2n-1)!! & n \text{ is positive}\\ [(-1)^{-n}(-2n-1)!!]^{-1} & \text{otherwise.}\end{cases}$$

Expansions (7) and (9) require a significantly fewer nested, as well as external, (l,m) sums, so the calculations are not intensive. Thus, we use Eqs. (7) and (9) to calculate the contribution of the overlapping atomic charge density (or potentials) arising from the near-neighbor sites onto the central site and whose total is given by

$$f_{\text{total}}(\mathbf{r}) = f_{\text{site}}(\mathbf{r}) + \sum_{\mathbf{R}\in \text{n.n.}} f_{\text{neigh}}(\mathbf{r}-\mathbf{R}). \tag{11}$$

With a sum in Eq. (11) over (at most) the first two shells of neighbors, the resulting sum of Eqs. (7) and (9) is a very numerical efficient form of Löwdin's approach. We use Eq. (11) to get the total, site-centered, charge density and find the site-dependent saddle points and SPR. In fact, the monopole $(l=0)$ terms in Eq. (7) already determine the SPR to within $\frac{1}{4}\%$, further reducing the computation.

First, we use $v(\mathbf{r}-\mathbf{R})$ as f in Eqs. (1) and (2) and Eq. (11), and we find a starting potential via the Herman-Skillman approach.[1] [We store and use $rv(\mathbf{r})$ as there are no Coulomb singularities.] Then, with $\rho(|\mathbf{r}-\mathbf{R}|)$ as f, we estimate the density and we use numerical gradients to find its saddle points rapidly. [We store $4\pi r^2\rho(|\mathbf{r}-\mathbf{R}|)$ as it is zero at the origin and positive definite elsewhere.] For ordered systems, it is straightforward for all sites in the unit cell to locate the saddle points by tracing the charge density along the lines connecting the nearest-neighbor atoms and assign this as the optimal MT radius. For example, for 16 atoms/cell the Herman-Skillman densities and potentials, Löwdin potential, SPR, and ASA radii are found in less than 0.5 s on 2005 Intel processor.

ASA cells and disordered alloys

These MT-SPR provide the Voronoi cells (Sec. I). Moreover, the interstitial density and potentials are now better described by plane waves and, in close-packed, metallic systems, they are almost constant beyond the MT-SPR, as seen in Fig. 1. Hence, for ASA calculations, MT corrections[28,50,51] are now a better approximation to the interstitial contributions. Empty spheres can be used in more open structures to improve further the basis.

To obtain ASA radii, volume must be conserved (a constraint). But, ASA overlap should be considered, especially for large and small MT spheres. These are discussed in the Appendix, where we derive an equation that provides unique ASA radii with minimal overlap for any configuration, including the disordered phase within a single-site approximation. In the ordered case, each inequivalent sublattice s has only one atom type (α) occupying it and the concentration $(c_{\alpha,s})$ of which is either 1 or 0. For disordered alloy the scenario differs from that of the ordered one, because translational symmetry is obtained only after the configurational averaging is performed, due to the fact that on each inequivalent sublattice $0 \le c_{\alpha,s} \le 1$. Thus, the configurationally averaged ASA radii at a site depend on all possible local chemical environments, not just a single one as in the perfectly ordered case. Nonetheless, we follow a similar procedure as the ordered case to estimate the radii of a particular atom β by calculating the saddle points along the lines connecting the nearest-neighbor sites. That is, for each site on a sublattice s (as in the ordered case) you put an atom of type β and populate the neighboring sites by all possible species α that are permitted. After weighting the various SPR $R_{\beta,s}^{\alpha,s'}$ by the probability of having an α atom in that neighboring site and sublattice s', we use the minimum SPR for that environment, i.e., $\bar{R}_{\beta,s}=\min_{\forall s'}[\Sigma_\alpha c_{\alpha,s'} R_{\beta,s}^{\alpha,s'}]$, if there is no short-range order. Once the configurationally averaged MT saddle-point radii for each species and sublattices are evaluated, the ASA radii are determined by the roots of a simple cubic equation; see the Appendix.

III. COMPUTATIONAL DETAILS

Calculations were performed via Green's function multiple scattering theory[52,53] of Korringa, Kohn, and Rostoker (KKR). We used the KKR-CPA to include[54,55] the chemical and magnetic disorder in the electronic structure and energetics, all treated on equal footing, for multisublattices and multicomponents. The CPA permits us to address the paramagnetic (PM) state via the disordered local moment[56–62] state to include moment-orientational disorder. We also used the screened-CPA (scr-CPA) (Ref. 63) to incorporate more properly the metallic screening due to charge correlations in the local chemical environment and predict more accurate enthalpies and charges. To get initial potentials and MT-SPR within our KKR-CPA code,[64] we automated the expansions via the Herman-Skillman method[1] using a numerical doubling grid (with 1001 points and doubling the grid steps every 200, so there are five sets of grids). We employed the local spin density approximation (LSDA) to the density-functional theory exchange and correlation functionals, as parametrized by von Barth and Hedin,[65] for ferromagnetic (FM) and PM states. For the valence electrons, scalar-relativisitic effects are included as described by Koelling and Harmon,[66] but core electrons are treated fully relativistically. For the ASA, we include only electrostatic monopoles (Madelung energy) plus *muffin-tin corrections*[25,28,50,51] (MTC) to include the interstitial electron for better structural parameters. All results are reported for $L_{\max}=3$ (or s, p, d, and f symmetries). Charge self-consistency is obtained via contour integrations of the Green's functions in the complex energy plane, using a Gauss-Legendre semicircular contour with 18–24 energy points. At each complex energy, a Brillouin zone integration was performed using Monkhorst-Pack special k-point method,[67] (e.g., for four-atom cells, 20^3 (4^3) k points near the real axis (far in the complex or below zero energy), yielding changes in relative energies of less than 2 meV/atom.

In some cases literature does not provide equivalent comparisons to the present results. If not, we used a pseudopotential plane-wave method, as implemented in the Vienna *ab initio* simulation package (VASP),[68,69] with a projector augmented wave (PAW) basis[70] to yield accurate energy differences. We used generalized gradient approximation (GGA)[71] and/or LSDA. We used 350–400 eV energy cutoff for the plane-wave basis set and similar Brillouin zone meshes to KKR but 3 mRy smearing of the density of states. Conver-

gence of the total energies (forces) is less than 2 meV/atom (30 meV/Å). Also, we use Stuttgart LMTO code[72] with combined corrections (which can adjust ASA sphere sizes for ordered systems via saddle points in the spherical, Hartree-only potential) and compare its results to the present approach, where our results agree much better to that from full-potential methods.

Due to their importance in stability and thermodynamics, we will compare two types of energy difference: (i) the formation energy, i.e., the alloy energy relative to the concentration-weighted sum of the α constituent energies at their equilibrium volumes, or

$$\Delta E_f = E^{\text{alloy}}(V_0;\{R_\alpha\}) - \sum_{\alpha=1}^{S} c_\alpha E^\alpha(V_\alpha^0;R_\alpha^0), \tag{12}$$

and (ii) a planar defect energy, i.e., the energy per m defects in an N-atom cell relative to the undefected cell with a planar defect area of A_{def}, or

$$\gamma_{\text{def}} = \frac{E_{\text{def}}^{\text{alloy}}(N;\{R_\alpha\}) - E_0^{\text{alloy}}(N;\{R_\alpha\})}{mA_{\text{def}}}. \tag{13}$$

Defect energies are less dependent upon the exchange correlation and other approximations used due to inherent cancellations. Here the equations are written to convey that these energy differences depend on the MT-SPR or ASA radii (i.e., $\{R_\alpha\}$) used in the basis. Clearly, in the definition of ΔE_f, there is a different set of radii for the alloy $\{R_\alpha\}$ than that for the elements R_α^0, whereas, for the defect energy, the defected and undefected cases have the same composition and $\{R_\alpha\}$. Thus, variational behavior is expected from Eq. (13), as we show, but not from Eq. (12). So both will provide stringent comparison between equal-sphere and MT-SPR-sphere calculations. That is, one must know *a priori* the set of $\{R_\alpha\}$ that will produce an optimally correct ΔE_f because it cannot be chosen by direct variation. Also, while direct variation of γ_{def} versus $\{R_\alpha\}$ is possible, the calculations are computationally expensive, requiring several $\{R_\alpha\}$ each with many atoms per unit cell. We use a (011) c domain in $L1_0$ CoPt, requiring 24 atoms/cell to give converged values for γ_{cdb}^{011}, to show direct minimization with changes in sphere radii. Such defects are of direct interest in temperature-dependent defect formation in this magnetic storage alloy.

IV. RESULTS AND DISCUSSION

Our focus here is to show that the MT-SPR representation, specifically in the ASA, provides a dramatic improvement for energetics and structural properties, as well as site charges. As such, we have considered A_3B and AB alloys in fcc, bcc, and hcp lattices. Two systems having significant atomic size differences are addressed, namely, fcc CoPt (of interest for high-density magnetic storage) that orders from fcc (A1) into $L1_0$ at 1098 K, and bcc (A2) CrW that phase segregates below 1950 K, whose constituents are in the same column of the Periodic Table. There is limited calorimetry data (e.g., formation enthalpies), although phase transition temperatures and structural parameters are well established. In addition, we study hcp Ti_3Al, whose DO_{19} ground state[73–75] exhibits a large c/a distortion.[76,77] This distortion is not a consequence of large difference in atomic sizes, but rather the cell shape. In addition, DO_{19} is almost degenerate with cubic $L1_2$ within DFT.[78–83]

Generally, the term charge transfer is not uniquely defined as excess charge on a site depends on how space is partitioned. In LAPW, for example, only excess charge in the chosen MT spheres is often quoted. "Bader charge"[19,20] is more relevant but determined in nonconvex topological partitions.[17,18] Here, we consider the excess charge in the atomic spheres, where the spherical part of the local charge density is better represented with MT-SPR and the excess charges in the MT-SPR ASA spheres reflect this; that is, for systems composed of atoms within the same columns of the Periodic Table, such as CrW, charges should be closer to neutral.

Careful comparison has been done only twice between various approximations to the disordered phase,[84,85] i.e., CPA, structural inversion method (SIM), and special quasirandom structures (SQS). The KKR-CPA [which includes (off-)diagonal disorder and multibody effects] performs an approximate configurational average concomitant with the charge self-consistency (scr-CPA adds local charge correlations[63]). The SIM (Refs. 86–89) attempts to construct an effective cluster expansion[90,91] to represent all configurations using enthalpies from a set of ordered configurations; if done correctly, then the SIM agrees with the CPA.[84] The SQS approximates (within a range smaller than the cell) the pair correlations in a fully disordered alloy from a perfectly ordered arrangement of atoms, in large (sometimes multiple) unit cells[92–95] that can experience large relaxations. The SQS assumes that there are no multibody correlations determining energetics, which could be important in the disordered phase.[84] Johnson and Asta[85] showed that if all methods used the same L_{max}, exchange correlation, etc., then each approximation gave similar results in systems with pair dominant interactions and similar sized atoms. We include SQS-N (N-atom, ordered layered cells) results for comparison to the faster one-atom-per-cell CPA results.

A. fcc CoPt

With large coercive fields and high magnetoanisotropy, FM-$L1_0$ CoPt-type alloys are candidates for high-density, magnetic storage media down to nanosize scale.[96] However, tetragonal (c/a) distortions inherent in the $L1_0$ compounds result in competition of the FM and anti-FM states,[97] decreasing the stability of the FM state with smaller system size. Thus, the relative stability of the ordered, disordered, and defected phases is key to the thermodynamic, structural, and magnetic properties. For example, when ordering below 1098 K (from PM-A1 to PM-$L1_0$), planar defects appear in micrographs,[98] such as c-domain and antiphase boundaries, then, subsequently, a Curie transition occurs at 723 K to FM-$L1_0$. Both of these transitions affect energy and formation of defect. Hence, the ΔE_f and planar defect energies, like γ_{cdb}^{011}, are of technological importance. Therefore, we focus on the PM-A1 and FM-$L1_0$ CoPt, both energy and structural properties, and show that the MT-SPR representation

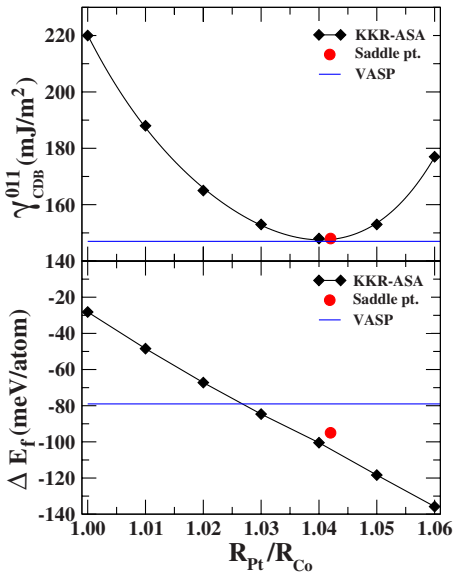

FIG. 2. (Color online) For $L1_0$ CoPt, (upper) γ^{011}_{cdb} (in mJ/m^2) and (lower) ΔE_f (in meV/atom) versus ratio of ASA radii R_{Pt}/R_{Co}. KKR-ASA: direct variation (diamonds) and SPR calculation (circle), and VASP (horizontal line). Direct variation finds optimal R_{Pt}/R_{Co} of 1.040 versus *a priori* SPR value of 1.042. The SPR-ASA γ^{011}_{cdb} is 148 versus 147 mJ/m^2 from VASP, whereas equal sphere is 220 mJ/m^2.

provides a remarkable improvement. In the A1 phase, by definition in Eq. (13), γ^{011}_{cdb} is zero.

In Fig. 2 for FM-$L1_0$ CoPt, we show the direct variation of ΔE_f and γ^{011}_{cdb} versus R_{Pt}/R_{Co} (the ratio of ASA radii). As expected, γ^{011}_{cdb} is variational, with a minimum of 148 mJ/m^2 at 1.040, substantially less that 220 mJ/m^2 at 1.0. The MT-SPR from Eqs. (7) and (9) gives the ratio to be 1.042 yielding γ^{011}_{cdb} of 148 mJ/m^2 also, the optimal value. The direct variation was obtained from several 24-atoms/cell calculations, whereas the MT-SPR were obtained *a priori* and a single calculation performed. While no experimental value of γ^{011}_{cdb} is available, the VASP value is 147 mJ/m^2, confirming the MT-SPR ASA value.

As shown in Fig. 2, $\Delta E_f^{L1_0}$ varies dramatically (but linearly) with R_{Pt}/R_{Co}, from −28 meV/atom at the ratio 1.0 to −100 meV/atom at 1.04 (a factor of 3 decrease). For the MT-SPR basis, it is −95 meV/atom, now in better comparison to VASP. In this case, the touching MT-SPR, which sum to $a_0\sqrt{2}/2$, are 1.3861 and 1.2908 Å (ratio 1.074) for Pt and Co, respectively, and the ASA radii are 1.5083 and 1.4475 Å (ratio 1.042), for ~10% overlap. (Using the Stuttgart LMTO code[72] based on the saddle points in the spherical potentials, we obtained −64 meV, where the MT radii were 1.3165 and 1.3378 Å leading to ASA radii of 1.459 and 1.482 Å for Co and Pt, respectively.)

More surprisingly, as shown in Table I, the FM-A1 ΔE_f^{dis} (scr-CPA) phase segregates (80 meV/atom) with equal spheres, whereas it mixes (−70 meV/atom) for MT-SPR case. The MT-SPR in this case are 1.41 and 1.2589 Å (ratio 1.12), which give ASA radii of 1.52 and 1.4545 Å (ratio 1.045). The change in sign for A1-CoPt is consistent with that found by Singh and Gonis[36] for NiPt when they adjusted spheres to charge-neutral case. This dramatic swing in ΔE_f^{dis} arises due to representing charge density better, but does not require that the sphere be arbitrarily chosen as charge neutral.

Besides being in agreement with VASP results, the FM $L1_0$ and A1 ΔE_f using the SPR-ASA are now consistent with known measurements[99,100] (made above the Curie point) in sign and magnitude; see Table I. (In recent calorimetry measurements on transition-metal binaries, it has been found that ΔE_f values are in closer agreement to DFT than the older values;[104–106] however, there have been no new measurements on Co-Pt systems, even with the renewed interest in these systems.) Our results in Table I are also in agreement with well-known models due to Miedema and co-workers[101] and CALPHAD (Ref. 102); in fact, our FM $L1_0$ and A1 ΔE_f are a constant shift of about 16 meV from those PM results.

Besides dramatically improving the calculated ΔE_f, the SPR shows, as expected, far less sensitivity to the L_{max} used within the spheres; see Table II for FM CoPt. Ordered and disordered SPR ΔE_f lower slightly versus L_{max}, as might be expected keeping only monopole terms. However, the ordering energy (E^{ord}, i.e., the difference in ordered and disordered energies) versus L_{max} remains unchanged, in contrast to the non-SPR basis. All systems studied thus far show similar behavior. Moreover, this behavior will lead to a reduction, e.g., in combined corrections in the LMTO-ASA. Of course, with full VP integration using the MT-SPR, there will be no need for any approximate corrections.

The FM-$L1_0$ magnetic moments for Co and Pt MT-SPR spheres are 1.75 and 0.38 μ_B (2.13 μ_B/cell), respectively, and 1.86 and 0.38 μ_B for equal spheres (2.24 μ_B/cell); compare these to the VASP (2.10 μ_B/cell) and 1.7 and 0.25 μ_B (1.95 μ_B/cell) from the neutron-scattering results of Cable, as discussed by van Laar[107] when reporting his magnetization measurements (1.90 μ_B/cell). With equal spheres, LMTO-ASA using combined corrections and $L_{max}=2$ found 1.85 and 0.38 μ_B (2.23 μ_B/cell),[108] the same as our equal sphere results. ASW-ASA calculations[32] found 1.69 and 0.37 μ_B using the experimental lattice parameters with no energies reported; however, they fixed the Co spheres from elemental hcp-Co results and then adjusted only Pt spheres to conserve volume (due to sensitivity of results on sphere sizes). Clearly, such a choice helps make Co spheres more Co like, but it is again not unique nor does it change with environment or composition, in contrast to our automated MT-SPR choice.

In Table III, we consider the local excess charge within the ASA spheres. For transition-metal atoms within the same column of the Periodic Table, one expects little charge transfer, where the ordering is made favorable from band hybridization, as quantified in NiPt.[109] Electronegativity of Pt (2.20) and Co (1.88) suggest that charge should transfer from Co to Pt. In the A1 phase, excess charge should be only slightly different, whereas, in $L1_0$, an increase occurs due to Madelung effects. In Table III, there is a change in sign of (and drop in magnitude by roughly a factor of 2) the excess charge between equal and MT-SPR spheres. Thus, in the MT-SPR ASA (Wigner-Seitz), the excess charges are now more what is expected from the electronegativities.

For disordered metals, the scr-CPA better reproduces the impurity screening arising from the charge correlations in the

TABLE I. KKR-ASA ΔE_f (in meV/atom) for (dis)ordered alloys with equal and SPR spheres, relative to elements in parent phase of alloy, for FM A1 and $L1_0$ CoPt, A2 and B2 CrW, A3 and $DO_{19}Ti_3Al$. Disorder is handled by (scr-)CPA. Other theory and experimental results are given for comparison including unrelaxed SQS.

		Equal sphere		SPR sphere	
Alloy	Method	ΔE_f^{ord}	ΔE_f^{dis}	ΔE_f^{ord}	ΔE_f^{dis}
	KKR-CPA	−28	155	−95	−65
	KKR-scr-CPA	−28	80	−95	−70
	KKR-SQS-$\bar{8}$ [a]		96		−66 [a]
	Expt.[b] (Ref. 99)			−140 ± 22	−129 ± 26
CoPt	Expt. (assess.)[b] (Ref. 100)				−102 ± 26
	Miedema (Ref. 101)			−114	
	CALPHAD (Ref. 102)				−88
	VASP			−79	
	VASP-GGA			−89	
	KKR-CPA	51	446	31	97
	KKR-scr-CPA	51	324	31	62
	KKR-SQS-8		344		55
CrW	KKR-SQS-16		379		116
	CALPHAD (Ref. 102)				82
	LAPW (Ref. 103)			33	
	LAPW-GGA (Ref. 103)			23	
	TB (Ref. 78)/EAM (Ref. 81)				110
	KKR-scr-CPA	−276	−161	−279	−146
Ti_3Al	Expt. (Refs. 73 and 74)			−273 ± 10 [c]	
	LAPW (Ref. 79), LASTO (Ref. 82)			−280 [d]	
	LAPW-GGA (Ref. 83)			−300	

[a]Average of two layered cells (Ref. 93) 8a (−334.6 meV) and 8b (+210.3 meV).
[b]$L1_0$ phase at 914 K and A1 at 1273 K (1173 K for assessed).
[c]$\Delta E_f^{DO_{19}}$ is average of −260, −290, and −270(±10) meV, respectively.
[d]$\Delta E_f^{L1_2}$ is −270 (LAPW), −280 (LASTO) vs −277 meV (KKR).

local environmental averaging.[63] This is evident in Table I where the CPA is compared with the scr-CPA. For equal spheres there is a large excess charge on all smaller atom sites (see Table III) from the tails of the charge density of the larger atom that have been arbitrarily cutoff at the smaller radii. Hence, the effect of screening should be much bigger; and, indeed, the ΔE_f drops by almost a factor of 2, from 155 to 80 meV/atom, but still remains positive. Whereas, for the MT-SPR basis, the MT sphere reflect more appropriately the extent of the charge density (see Table III) and the effect of the screening is substantially less, from −67 to −70 meV/atom, and now A1-CoPt is stable at high temperatures, as observed.

TABLE II. KKR-ASA ordered and scr-CPA ΔE_f and E^{ord} for CoPt (in meV/atom) vs $L_{\max}$ with equal and MT-SPR spheres, showing less sensitivity to $L_{\max}$ with MT-SPR basis.

	Equal sphere			SPR sphere		
$L_{\max}$	ΔE_f^{ord}	ΔE_f^{dis}	E^{ord}	ΔE_f^{ord}	ΔE_f^{dis}	E^{ord}
2	7	130	123	−91	−65	26
3	−28	80	108	−95	−70	25
4	−11	100	111	−107	−81	26

Table I also shows the results of SQS calculated at the scr-CPA lattice constant in Table IV. The A1 phase for 50% binary is approximated as an average of two, eight-atom configurations[93] that are layered along [113] in a sequence of $A_2B_3A_2B_1$. As a result, one must do two calculations (swapping A and B atoms) and average them. These two configurations can be dramatically different in energy, as we find for FM CoPt; see footnote in Table I. Of course, the SQS-8 results, because they are layered cells, may exhibit very different relaxations for each sequence; and any internal relaxations, which can be significant,[94] will move the SQS-8 toward the scr-CPA results. We note that a comparison of SQS and CPA with equal spheres has been done before,[114] although not using the same code nor approximations. The SQS usually agreed with the much faster CPA, except in cases where there were large differences in the size of the

TABLE III. Excess ASA charges, large atom (first line) and small atom (second line) for (dis)ordered alloys with equal and SPR spheres for same systems as in Table I.

		Equal sphere		SPR sphere	
System	Method	ΔQ_f^{ord}	ΔQ_f^{dis}	ΔQ_f^{ord}	ΔQ_f^{dis}
	KKR-CPA		−0.113		+0.058
			+0.113		−0.058
CoPt	KKR-scr-CPA	−0.277	−0.187	+0.163	+0.049
		+0.277	+0.187	−0.163	−0.049
	KKR-CPA		−0.352		−0.090
			+0.352		+0.090
CrW	KKR-scr-CPA	−0.662	−0.581	+0.162	−0.150
		+0.662	+0.581	−0.162	+0.150
Ti_3Al	KKR-scr-CPA	+0.222	+0.108	+0.216	−0.069
		−0.074	−0.036	−0.072	+0.023

atoms. Present results show that it was due to representation and not the CPA.

Trends in lattice constants are also better reproduced. In Table IV, for the observed FM phase, a^{ord} (c/a) is 3.80 Å (0.972), compared to our calculated value of 3.784 Å (0.984). We find a^{dis} is 3.78 Å for the PM-A1 phase (in parenthesis in Table IV), compared to measured value of 3.81 Å. All our results are within the expected 0.5%–1.5% LSDA error. Notice that for fictitious FM-A1 phase we find a much smaller a^{dis} of 3.740 Å for the scr-CPA, so it is critical to address more properly the A1-CoPt PM state. In particular, the change in a_0 from A1 to $L1_0$ is correctly reproduced. Also, the $L1_0$ volume [i.e., $(c/a)a^3$] is the same for both theory and experiment. Thus, MT-SPR results compare significantly better to the experiment for both the ordered and disordered, especially for the scr-CPA that properly takes into account the effect of charge correlation in the local environment. So past errors involving CPA calculations were not due to an error in CPA description but the representation of the density and potential.

B. bcc CrW

The A2 $Cr_{50}W_{50}$ exhibits segregation below 1950 K. To compare with other methods, we calculated the fictitious B2 CrW, and SQS-8 and SQS-16 (unrelaxed) approximations to A2 phase at the a_0 from scr-CPA. The MT-SPR for B2 find that W is 14% larger than Cr, i.e., R_W/R_{Cr} is 1.14, see Fig. 1,

TABLE IV. KKR-ASA (T=0 K) and room temperature (RT) measured lattice parameters a (in Å) and c/a (second line) for (dis)ordered alloys from equal and SPR spheres for systems given in Table I. For A1-CoPt, there is a lattice constant for FM (PM) state. Experimental results are taken from Refs. 110 and 111 for CoPt, Refs. 112 and 113 for CrW, and Refs. 76 and 77 for Ti_3Al.

		Equal sphere		SPR sphere		Expt.		Other theory
System	Method	a_{ord}	a_{dis}	a_{ord}	a_{dis}	a_{ord}	a_{dis}	a_{ord}
	KKR-CPA		3.70 (3.720)		3.726 (3.793)			
			1.00		1.00			
CoPt	KKR-scr-CPA	3.75	3.72 (3.735)	3.784	3.740 (3.780)	3.80	n/a(3.81) [a]	3.746[b]
		0.988	1.00	0.984	1.00	0.972	1.00	0.967[b]
	KKR-CPA		3.04		3.013			
			1.00		1.00			
CrW	KKR-scr-CPA	3.09	3.03	3.016	3.011		3.043[c]	2.98[d]
		1.00	1.00	1.00	1.00		1.00	1.00[d]
Ti_3Al	KKR-scr-CPA	3.001	3.019	3.007	3.019	3.053 (3.059)		3.001[d]
		0.803	0.803	0.803	0.803	0.801 (0.803)		0.807[d]

[a]1100 K PM phase with $a \sim 3.81$ extrapolated to RT gives $a \sim 3.77$ (Ref. 111).
[b]VASP-LDA results: this work for $L1_0$ CoPt.
[c]At 1700 K, two-phase quenched values are unchanged (Ref. 113).
[d]FLAPW-LDA results: Ref. 103 for B2 CrW and Ref. 79 for $DO_{19}Ti_3Al$.

compared to 1.077 in the A2 (scr-CPA) phase.

For B2 CrW, Table I shows that the energy from the SPR basis is significantly improved compared to equal sphere, with ΔE_f of 31 meV versus 33 meV in LAPW. (From the Stuttgart LMTO code,[72] we find 6 meV from their MT radii of 1.2147 and 1.3976 Å, which lead to ASA radii of 1.3745 and 1.5815 Å for Cr and W, respectively.) Empirical modeling by Miedema and co-workers[101] found 10 meV for the B2 phase. Even more dramatic is the effect on energy and structure in the observed A2 phase. For equal spheres, $\Delta E_f^{\mathrm{dis}}$ is 324 meV (446 meV) in scr-CPA (CPA), due to the large (unphysical) excess charges in the spheres given by the bad representation of density. In contrast, for the SPR representation, $\Delta E_f^{\mathrm{dis}}$ is 62 meV (97 meV) for the scr-CPA (CPA) in Table I; the SQS-8 $\Delta E_f^{\mathrm{dis}}$ gives a similar result. The SQS-16 is significantly larger than the scr-CPA or SQS-8, perhaps relaxations may lower $\Delta E_f^{\mathrm{dis}}$ in this many layered cell. For A2 CrW, 110 meV were reported for tight-binding[78] and embedded atom[81] methods, see Table I, again too large. CALPHAD modeling[102] found 82 meV, but based on phase diagram fitting rather than enthalpy data.

How good is our SPR-based A2 result? As no enthalpy data is available, we use a mean-field estimate for the critical temperature (i.e., $k_B T_c \sim 2\Delta E_f^{\mathrm{dis}}/\Delta S$, where ΔS is point entropy), validated in Ref. 115 as accurate for alloys with no topological frustration. We obtain 2079 K for $Cr_{50}W_{50}$ from the MT-SPR scr-CPA result, compare to the observed 1950 K, and verifying the quantitative improvement for the SPR basis.

The trends in the lattice constants and charges are also better reproduced. In Table IV, the MT-SPR scr-CPA result gives a^{dis} of 3.011 Å compared to a^{ord} of 3.043 Å. Notably, the MT-SPR lattice constant is less than experiment, as expected within LDA, in contrast to the equal sphere case. Similarly, for the B2 phase, a^{ord} is 3.016 Å, which also compares better to LAPW (2.98 Å).

In Table III, the excess charges in the MT-SPR ASA spheres now exhibit the physically expected more neutral spheres, in contrast to the equal sphere case. Also, the sign of the excess charges in ordered B2 has changed and now reflects the sign expected from electronegativities of W (1.70) versus Cr (1.66), i.e., more charge on W. For A2 CrW, although spheres are much more charge neutral, the excess charge does not have the same sign as B2 because they have slightly smaller radii than B2, reflecting the various environments in the configuration average, giving 62 meV for $\Delta E_f^{\mathrm{dis}}$. In contrast, fixing the radii of A2 to that of B2 increases the $\Delta E_f^{\mathrm{dis}}$ to 91 meV/atom, for a 50% increase to the critical temperature, in disagreement with experiment. The excess charges in A2 versus B2 reflect the changes in the saddle points going from an averaged to a single environment (see below).

It is worth again comparing the MT or ASA radii. In the fictitious B2 phase, the MT-SPR are 1.4238 and 1.1952 Å (ratio 1.191) for W and Cr, respectively. The ASA radii are then 1.5781 and 1.3790 Å (ratio 1.144). Clearly in Fig. 1, the origin for the energy improvements arises from adjusting the MT radii to the saddle points to better represent the charge density distribution around a site. More interesting are the radii in the observed A2 phase, especially since the excess charge has dramatically changed. The MT-SPR are 1.360 and 1.2308 Å (ratio 1.105) for W and Cr, respectively. The ASA radii are then 1.535 and 1.4253 Å (ratio 1.077).

For completeness, adjusted-ASA KKR-CPA calculations[116] were done early on by varying $\Delta E_f^{\mathrm{CPA}}$ with respect to $R_{\mathrm{big}}/R_{\mathrm{small}}$ while conserving volume and a minimum was found for charge-neutral spheres. The same result cannot be found in ordered phase because $\Delta E_f^{\mathrm{ord}}$ is not variational versus $R_{\mathrm{big}}/R_{\mathrm{small}}$; see Fig. 2. (Clearly, this is not the same as finding the MT-SPR and approximating the Voronoi polyhedra by the ASA, as done in Fig. 2.) This charge-neutral-CPA method was abandoned because the (fictitious) variational behavior was due only to the single-site approximation and the use of the ASA.[116] That is, for A2 CrW, with similar bulk moduli, Cr and W spheres trade off charge to eliminate the electrostatic contribution to the formation energy and put it into band energy within a single site. One could make an arbitrary choice for $R_{\mathrm{big}}/R_{\mathrm{small}}$, such as assuming the charge-neutrality condition for all configurations.[36] However, for alloys with constituents having dissimilar bulk moduli (see end of Sec. I), charge neutrality gives unphysical results, as in Al-Li.[36,116] The $R_{\mathrm{big}}/R_{\mathrm{small}}$ are different in the ordered and disordered phases, and only the MT-SPR ASA properly reflects their different bonding characteristics, giving unique and optimal description, as for A2 and B2 CrW.

C. hcp Ti_3Al

$DO_{19}Ti_3Al$ is included to show that even slight changes in MT-SPR lead to improvements in comparison to LAPW and experiment. The energetics are subtle, with DFT showing that DO_{19} is almost degenerate with $L1_2$.[78–83] The SPR basis gives a slight reduction of 3 meV/atom, closer to LAPW. The ASA (FLAPW) ΔE_f is −279 meV (−280 meV) for DO_{19}, in agreement with experiment; see Table I. We find $L1_2$ only 2 meV higher than DO_{19}, whereas FLAPW finds 10 meV higher.[79] LASTO and LMTO find them as degenerate.[79,82,83] Hence, even though the changes in ASA sphere sizes are small ($R_{\mathrm{Al}}/R_{\mathrm{Ti}}=1.0022$), the SPR basis does improve the results. A similar reduction of 2 meV/atom is found for $L1_2$ from equal to MT-SPR ASA, leaving the DO_{19}-$L1_2$ energy difference unchanged. The A3 phase is also predicted to be stable.

The a_0 from MT-SPR ASA are within 1.7% from experiment[76,77] and 0.3% from the full-potential results,[79] and c/a agrees with experiment; see Table IV. Similarly, excess charges have little changes and in accord with Al being more electronegative than Ti, except for the A3 phase where the sign changes on Al. This finding indicates that the average A3 environment does not favor the same (electrostatic) charge effects as DO_{19} and that the ordering is much more favored, as evident in Table I.

V. CONCLUSION

Many electronic-structure methods use site-centered expansions of density and potential inside nonoverlapping, "muffin-tin" (MT) spheres with an interstitial basis set. We

have presented a numerically fast, site-shifted (spherical harmonic) expansion of density to determine, before any calculation, the radii of the saddle points (SPR) in the total density at each site using only the *overlapping atomic charge density*, easily implemented via standard Herman-Skillman atomic-type calculations, for arbitrary number of sublattices and alloying components, and for ordered and (CPA) disordered alloys. The MT spheres given by the SPR in the total density reflect the boundary separating the spherical and nonspherical density between neighboring atoms, and, therefore, give the optimal region for expanding in spherical harmonics, as we verified by direct variation.

We adapted the MT-SPR basis to the KKR-CPA in the atomic sphere approximation (ASA) to study ordered and disordered alloys with large atomic size differences. We found that formation energies and structural parameters are in strikingly better agreement with more exact *ab initio* or experimental results, with no increase in computational cost, and there is a much reduced sensitivity of the results on the assumed angular momentum cutoff. Moreover, the excess charges on a site are now more those expected from electronegativity. In the case of CPA, the SPR basis provides reliable values, resolving outstanding issues; we showed that former bad (or inconsistent) CPA results were not due to the approximation itself but to the use of poorly represented densities and potentials. For general systems, due to these improvements from the SPR basis, we now can predict accurately the ordered, partially ordered, and fully disordered states in the same code. Finally, we note that the MT-SPR also uniquely guarantee convex, weighted Voronoi polyhedra that may be found rapidly, permitting full integration over each polyhedra via isoparametric integration, which we are now implementing.

ACKNOWLEDGMENTS

We acknowledge grants from the Department of Energy (Grant No. DEFG02-03ER46026) and Lawrence Livermore National Laboratory (Grant No. B573247) to Illinois. D.D.J. also acknowledges support from Grant No. DMR-0705089 from the National Science Foundation.

APPENDIX: CALCULATION OF ASA RADII

Assume N_s sublattices and α_s number of components in each of the s sublattices in the unit cell. If V is the volume of the unit cell, volume conservation within an ASA calculation demands

$$V = \frac{4}{3}\pi \sum_{s=1}^{N_s} \sum_{\alpha=1}^{\alpha_s} c_{\alpha,s} [R_{\alpha,s}^{\mathrm{ASA}}]^3 n_s, \tag{A1}$$

where n_s is atomic degeneracy, and $c_{\alpha,s}$ and $R_{\alpha,s}^{\mathrm{ASA}}$ are the concentration and ASA radii of the α atom at the s sublattice.

If $R_{\alpha,s}^{\mathrm{MT}}$ are the calculated MT radii for the atom α on the sublattice s, then we have

$$R_{\alpha,s}^{\mathrm{ASA}} = R_{\alpha,s}^{\mathrm{MT}} + \Delta R_{\alpha,s}, \tag{A2}$$

where $\Delta R_{\alpha,s}$ is increment to a MT radii to get a volume-conserving ASA radii, which depend on both α and s. Let us denote the smallest of $\{R_{\alpha,s}^{\mathrm{MT}}\}$ as R_{ref}, i.e., $R_{\mathrm{ref}} \leq R_{\alpha,s}^{\mathrm{MT}}$ $(\forall \alpha, s)$. For mathematical convenience we define the ratio

$$\frac{R_{\alpha,s}^{\mathrm{MT}}}{R_{\mathrm{ref}}} = X_{\alpha,s}. \tag{A3}$$

At this point, a choice has to be made to conserve volume. First, we could equally scale all spheres, fixing the only remaining single parameter; however, the largest $R_{\alpha,s}^{\mathrm{MT}}$ will increase radially the most (increasing the ASA overlap error more). Second, noting that smaller atoms surrounded by large atoms have more interstitial around them, we could impose a restriction on the increment $\Delta R_{\alpha,s}$ such that the larger atoms expand less as compared to the smaller ones; an efficient and physical means to minimize the overlap between two very different sized atoms. We use the second approach, which can be formulated by the condition that

$$\frac{\Delta R_{\alpha,s}}{\Delta R_{\mathrm{ref}}} = \frac{1}{X_{\alpha,s}}, \tag{A4}$$

i.e., $\Delta R_{\alpha,s} \propto (R_{\alpha,s}^{\mathrm{MT}})^{-1}$. Using Eqs. (A2)–(A4) in Eq. (A1), we get

$$V = A + B(\Delta R_{\mathrm{ref}}) + C(\Delta R_{\mathrm{ref}})^2 + D(\Delta R_{\mathrm{ref}})^3 \tag{A5}$$

with coefficients

$$A = \frac{4\pi}{3} R_{\mathrm{ref}}^3 \sum_{\alpha,s} n_s c_{\alpha,s} X_{\alpha,s}^3,$$

$$B = 4\pi R_{\mathrm{ref}}^2 \sum_{\alpha,s} n_s c_{\alpha,s} X_{\alpha,s},$$

$$C = 4\pi R_{\mathrm{ref}} \sum_{\alpha,s} n_s c_{\alpha,s} X_{\alpha,s}^{-1},$$

$$D = \frac{4\pi}{3} \sum_{\alpha,s} n_s c_{\alpha,s} X_{\alpha,s}^{-3}. \tag{A6}$$

Because we know all $\{R_{\alpha,s}^{\mathrm{MT}}\}$, all the $X_{\alpha,s}$ are known, as are all of $c_{\alpha,s}, n_s$ and V, and so we can solve Eq. (A5) for ΔR_{ref}. Once ΔR_{ref} is evaluated, Eq. (A4) can be used to calculate the increment $\{\Delta R_{\alpha,s}\}$ and, hence, $\{R_{\alpha,s}^{\mathrm{ASA}}\}$ from Eq. (A2). If the alloy is ordered, $c_{\alpha,s}$ are 1 on each sublattice, otherwise this is a single-site average.

[1] F. Herman and S. Skillman, *Atomic Structure Calculations* (Prentice-Hall, Englewood Cliffs, NJ, 1954).
[2] P.-O. Löwdin, Adv. Phys. **5**, 1 (1956).
[3] G. Voronoi, J. Reine Angew. Math. **134**, 198 (1908).
[4] B. J. Gellatly and J. L. Finney, J. Non-Cryst. Solids **50**, 313 (1982).
[5] B. J. Gellatly and J. L. Finney, J. Mol. Biol. **161**, 305 (1982).
[6] F. Aurenhammer, SIAM J. Comput. **16**, 78 (1987).
[7] S. C. van der Marck, Phys. Rev. Lett. **77**, 1785 (1996).
[8] S. Sastry, D. S. Corti, P. G. Debenedetti, and F. H. Stillinger, Phys. Rev. E **56**, 5524 (1997).
[9] V. A. Luchnikov, N. N. Medvedev, L. Oger, and J.-P. Troadec, Phys. Rev. E **59**, 7205 (1999).
[10] F. Aurenhammer and H. Edelsbrunner, Pattern Recognit. **17**, 251 (1984).
[11] H. Edelsbrunner, *Algorithms in Combinatorial Geometry* (Springer-Verlag, New York, 1987).
[12] H. Edelsbrunner and N. R. Shah, Algorithmica **15**, 223 (1996).
[13] A. Gonis, *Green Functions for Ordered and Disordered Systems* (Elsevier Science Publishers, Amsterdam, 1992).
[14] J. Zabloudil, R. Hammerling, L. Szunyogh, and P. Weinburger, *Electron Scattering in Solid Matter: A Theoretical and Computational Treatise* (Springer-Verlag, Berlin, 2005).
[15] N. Stefanou, H. Akai, and R. Zeller, Comput. Phys. Commun. **60**, 231 (1990).
[16] N. Stefanou and R. Zeller, J. Phys.: Condens. Matter **3**, 7599 (1991).
[17] R. F. W. Bader, *Theory of Atoms in Molecules* (Oxford University Press, Oxford, 1990).
[18] P. F. Zou and R. F. W. Bader, Acta Crystallogr. A **50**, 714 (1994).
[19] G. Henkelman, A. Arnaldsson, and H. Jónsson, Comput. Mater. Sci. **36**, 354 (2006).
[20] E. Sanville, S. D. Kenny, R. Smith, and G. Henkelman, J. Comput. Chem. **28**, 899 (2007).
[21] C. F. Guerra, J.-W. Handgraaf, E. J. Baerends, and F. M. Bickelhaupt, J. Comput. Chem. **25**, 189 (2004).
[22] Javier Bernal, FORTRAN codes for Voronoi tesselation and Delauney triangulations, NIST Math webpages (http://math.nist.gov/JBernal/JBernal_Sft.html).
[23] J. Bernal, National Institute of Standards and Technology Internal Report No. 4321, 1990 (unpublished).
[24] O. K. Andersen, Phys. Rev. B **12**, 3060 (1975).
[25] D. Glötzel, B. Segall, and O. K. Andersen, Solid State Commun. **36**, 403 (1980).
[26] A. Bratkovsky and S. Y. Savrasov, J. Comput. Phys. **88**, 243 (1990).
[27] S. Kobayashi and T. Fujiwara, Phys. Rev. B **55**, 7445 (1997).
[28] A. K. McMahan, Phys. Rev. B **30**, 5835 (1984).
[29] C. Amador, W. R. L. Lambrecht, and B. Segal, MRS Symposia Proceedings No. 253 (Materials Research Society, Pittsburgh, 1992), p. 297.
[30] K.-i. Masuda-Jindo and K. Terakura, Phys. Rev. B **39**, 7509 (1989).
[31] J. Hafner, *From Hamiltonians to Phase Diagrams* (Springer-Verlag, Berlin, 1987).
[32] A. Kootte, C. Haas, and R. A. de Groot, J. Phys.: Condens. Matter **3**, 1133 (1991).
[33] R. Magri, S.-H. Wei, and A. Zunger, Phys. Rev. B **42**, 11388 (1990).
[34] J. Kudrnovsky, S. K. Bose, and O. K. Andersen, Phys. Rev. B **43**, 4613 (1991).
[35] P. A. Korzhavyi, A. V. Ruban, S. I. Simak, and Yu. Kh. Vekilov, Phys. Rev. B **49**, 14229 (1994).
[36] P. P. Singh and A. Gonis, Phys. Rev. B **49**, 1642 (1994).
[37] O. K. Andersen, A. V. Postnikov, and S. Y. Savrasov, in *Applications of Multiple Scattering Theory to Materials Science*, edited by W. H. Butler, P. Dederichs, A. Gonis, and R. Weaver (Materials Research Society, Pittsburgh, 1992), Vol. 253, pp. 37–70.
[38] O. Jepsen and O. K. Andersen, Z. Phys. B: Condens. Matter **97**, 35 (1995).
[39] H. J. Silverstone, J. Chem. Phys. **47**, 537 (1967).
[40] N. Suzuki, J. Math. Phys. **25**, 1133 (1984).
[41] R. R. Sharma, J. Math. Phys. **9**, 505 (1968).
[42] R. R. Sharma, Phys. Rev. A **13**, 517 (1976).
[43] H. W. Jones and C. A. Weatherford, Int. J. Quantum Chem. **14**, Supplement 12, 483 (1978).
[44] I. I. Guseinov, J. Chem. Phys. **69**, 4990 (1978).
[45] R. A. Sack, J. Math. Phys. **5**, 245 (1964).
[46] R. A. Sack, J. Math. Phys. **5**, 252 (1964).
[47] R. A. Sack, Theoretical Chemistry Institute, University of Wisconsin Technical Report No. WIS-TCI-188, 1966 (unpublished).
[48] M. Geller, J. Chem. Phys. **36**, 2424 (1962).
[49] H. J. Silverstone, J. Chem. Phys. **45**, 4337 (1966).
[50] S. Asano and J. Yamashita, J. Phys. Soc. Jpn. **30**, 667 (1971).
[51] N. E. Christensen and S. Satpathy, Phys. Rev. Lett. **55**, 600 (1985).
[52] J. Korringa, Physica (Utrecht) **13**, 392 (1947).
[53] W. Kohn and N. Rostoker, Phys. Rev. **94**, 1111 (1954).
[54] D. D. Johnson, D. M. Nicholson, F. J. Pinski, B. L. Gyorffy, and G. M. Stocks, Phys. Rev. Lett. **56**, 2088 (1986).
[55] D. D. Johnson, D. M. Nicholson, F. J. Pinski, B. L. Gyorffy, and G. M. Stocks, Phys. Rev. B **41**, 9701 (1990).
[56] A. J. Pindor, J. B. Staunton, G. M. Stocks, and H. Winter, J. Phys. F: Met. Phys. **13**, 979 (1983).
[57] J. B. Staunton, B. L. Györffy, A. J. Pindor, G. M. Stocks, and H. Winter, J. Phys. F: Met. Phys. **15**, 1387 (1985).
[58] F. J. Pinski, J. B. Staunton, B. L. Györffy, D. D. Johnson, and G. M. Stocks, Phys. Rev. Lett. **56**, 2096 (1986).
[59] D. D. Johnson, F. J. Pinski, J. B. Staunton, B. L. Györffy, and G. M. Stocks, in *Physical Metallurgy of Controlled Expansion INVAR-type Alloys*, edited by K. Russell and D. Smith (The Minerals, Metals, and Materials Society, Warrendale, PA, 1989), pp. 3–24.
[60] J. B. Staunton, D. D. Johnson, and F. J. Pinski, Phys. Rev. Lett. **65**, 1259 (1990).
[61] D. D. Johnson and W. A. Shelton, in *The INVAR Effect—A Centennial Symposium*, edited by J. Wittenauer (The Minerals, Metals, and Materials Society, Warrendale, PA, 1997), pp. 63–74.
[62] V. Crisan, P. Entel, H. Ebert, H. Akai, D. D. Johnson, and J. B. Staunton, Phys. Rev. B **66**, 014416 (2002).
[63] D. D. Johnson and F. J. Pinski, Phys. Rev. B **48**, 11553 (1993).
[64] D. D. Johnson, A. Alam, and A. V. Smirnov, *MECCA: Multiple-Scattering Electronic-Structure Calculations for Complex Alloys (KKR-CPA Program, ver. 1.9)* (University of Illinois, Illinois, 2008).
[65] U. von Barth and L. Hedin, J. Phys. C **5**, 1629 (1972).
[66] D. D. Koelling and B. N. Harmon, J. Phys. C **10**, 3107 (1977).
[67] H. J. Monkhorst and J. D. Pack, Phys. Rev. B **13**, 5188 (1976).

[68] G. Kresse and J. Furthmüller, Phys. Rev. B **54**, 11169 (1996).
[69] G. Kresse and J. Furthmüller, Comput. Mater. Sci. **6**, 15 (1996).
[70] G. Kresse and D. Joubert, Phys. Rev. B **59**, 1758 (1999).
[71] J. P. Perdew and Y. Wang, Phys. Rev. B **45**, 13244 (1992).
[72] O. K. Andersen *et al.*, LMTO Package Stuttgart, Max-Planck-Institut Stuttgart webpages (http://www.fkf.mpg.de/andersen/).
[73] O. Kubaschewski and W. A. Dench, Acta Metall. **3**, 339 (1955).
[74] O. Kubaschewski and G. Heymer, Trans. Faraday Soc. **56**, 473 (1960).
[75] *Smithells Metals Reference Book*, 6th ed., edited by E. Brandes (Butterworths, London, 1983).
[76] W. B. Pearson, *A Handbook of Lattice Spacings and Structures of Metals and Alloys* (Pergamon, New York, 1958).
[77] R. Benedek, A. van de Walle, S. S. A. Gerstl, M. D. Asta, D. N. Seidman, and C. Woodward, Phys. Rev. B **71**, 094201 (2005).
[78] C. Colinet, A. Bessoud, and A. Pasturel, J. Phys. F: Met. Phys. **18**, 903 (1988).
[79] T. Hong, T. J. Watson-Yang, X.-Q. Guo, A. J. Freeman, T. Oguchi, and J.-h. Xu, Phys. Rev. B **43**, 1940 (1991).
[80] M. J. Mehl, Phys. Rev. B **47**, 2493 (1993).
[81] O. Yifang, Z. Bangwei, L. Shuzhi, and J. Zhanpeng, Z. Phys. B: Condens. Matter **101**, 161 (1996).
[82] R. E. Watson and M. Weinert, Phys. Rev. B **58**, 5981 (1998).
[83] R. R. Zope and Y. Mishin, Phys. Rev. B **68**, 024102 (2003).
[84] N. A. Zarkevich and D. D. Johnson, Phys. Rev. Lett. **92**, 255702 (2004).
[85] D. D. Johnson and M. D. Asta, Comput. Mater. Sci. **8**, 54 (1997).
[86] J. W. D. Connolly and A. R. Williams, Phys. Rev. B **27**, 5169 (1983).
[87] D. De Fontaine, Solid State Phys. **47**, 33 (1994).
[88] A. Zunger, in *Statics and Dynamics of Alloy Phase Transformations*, NATO ASI Series Vol. 319, edited by P. Turchi and A. Gonis (Plenum, New York, 1994), p. 361.
[89] D. D. Johnson, in *Encyclopedia of Materials: Science & Technology*, edited by K. H. J. Buschow *et al.* (Elsevier, New York, 2001).
[90] J. M. Sanchez, F. Ducastelle, and D. Gratias, Physica A **128**, 334 (1984).
[91] J. M. Sanchez, Phys. Rev. B **48**, 14013 (1993).
[92] A. Zunger, S.-H. Wei, L. G. Ferreira, and J. E. Bernard, Phys. Rev. Lett. **65**, 353 (1990).
[93] S.-H. Wei, L. G. Ferreira, J. E. Bernard, and A. Zunger, Phys. Rev. B **42**, 9622 (1990).
[94] M. H. F. Sluiter and Y. Kawazoe, Europhys. Lett. **57**, 526 (2002).
[95] C. Wolverton, Acta Mater. **49**, 3129 (2001).
[96] S. Sun, C. B. Murray, D. Weller, L. Folks, and A. Moser, Science **287**, 1989 (2000).
[97] G. Brown, B. Kraczek, A. Janotti, T. C. Schulthess, G. M. Stocks, and D. D. Johnson, Phys. Rev. B **68**, 052405 (2003).
[98] Y. Le Bouar, A. Loiseau, A. Finel, and F. Ducastelle, Phys. Rev. B **61**, 3317 (2000).
[99] R. Hultgren, P. D. Desai, D. T. Hawkins, M. Gleiser, and K. K. Kelley, *Selected Values of Thermodynamic Properties of Binary Alloys* (American Society for Metals, Metals Park, OH, 1973).
[100] J. P. Cyr, J. Dellacherie, and D. Balesdent, J. Chem. Eng. Data **26**, 174 (1981).
[101] F. R. de Boer, R. Boom, W. C. M. Mattens, A. R. Miedema, and A. K. Niessen, *Cohesion in Metals: Transition Metal Alloys* (North-Holland, New York, 1988), Vol. 19.
[102] P. Franke, D. Neushütz, and Scientific Group Thermodata Europe (SGTE), *Landolt-Börnstein: Group IV, 19B: Binary Systems*, Vol. 19B2 (Springer, Berlin, 2007).
[103] M. J. Mehl (private communication).
[104] O. J. Kleppa, J. Phase Equilib. **15**, 240 (1994).
[105] Q. Guo and O. J. Kleppa, J. Alloys Compd. **321**, 169 (2001).
[106] S. V. Meschel and O. J. Kleppa, J. Alloys Compd. **350**, 205 (2003).
[107] B. van Laar, J. Phys. France **25**, 600 (1964).
[108] A. Kashyap, K. B. Garg, A. K. Solanki, T. Nautiyal, and S. Auluck, Phys. Rev. B **60**, 2262 (1999).
[109] F. J. Pinski, B. Ginatempo, D. D. Johnson, J. B. Staunton, G. M. Stocks, and B. L. Gyorffy, Phys. Rev. Lett. **66**, 766 (1991).
[110] N. I. Vlasova, G. S. Kandaurova, and N. N. Shchegoleva, J. Magn. Magn. Mater. **222**, 138 (2000).
[111] C. Leroux, M. C. Cadeville, V. Pierron-Bohnes, G. Inden, and F. Hinz, J. Phys. F: Met. Phys. **18**, 2033 (1988).
[112] W. Trzebiatowski, H. Ploszek, and J. Lobzowski, Anal. Chem. **19**, 93 (1947).
[113] S.-V. Nagender Naidu, A. M. Sriramamurthy, P. Rama Rao, and T. B. Massalski, Anal. Chem. **2**, 1353 (1990).
[114] C. Jiang, C. Wolverton, J. Sofo, L.-Q. Chen, and Z.-K. Liu, Phys. Rev. B **69**, 214202 (2004).
[115] N. A. Zarkevich, T. L. Tan, and D. D. Johnson, Phys. Rev. B **75**, 104203 (2007).
[116] D. D. Johnson (unpublished).